ResearchGate

See discussions, stats, and author profiles for this publication at: https://www.researchgate.net/publication/24222289

# Detailed Atomistic Molecular Dynamics Simulations of α-Conotoxin AuIB in Water

**ARTICLE** *in* THE JOURNAL OF PHYSICAL CHEMISTRY B · MAY 2009

Impact Factor: 3.3 · DOI: 10.1021/jp806734c · Source: PubMed

CITATIONS
3

READS
28

**3 AUTHORS**, INCLUDING:

Martin Kröger
ETH Zurich
**239** PUBLICATIONS **3,836** CITATIONS

SEE PROFILE

Available from: Martin Kröger
Retrieved on: 26 January 2016

# Detailed Atomistic Molecular Dynamics Simulations of α-Conotoxin AuIB in Water

**Nikos Ch. Karayiannis and Manuel Laso***

*Institute for Optoelectronics and Microsystems (ISOM) and ETSII, Universidad Politécnica de Madrid (UPM), José Gutiérrez Abascal 2, E-28006 Madrid, Spain*

**Martin Kröger**

*Polymer Physics, ETH Zürich, Department of Materials, Wolfgang-Pauli-Strasse 10, CH-8093 Zürich, Switzerland*

*Received: July 29, 2008; Revised Manuscript Received: February 3, 2009*

We present results about the shape, size, structure, conformational stability, and hydrodynamics of α-conotoxin AuIB (a disulfide-rich peptide from the venom of *Conus aulicus*, recognized as a nicotinic acetylcholine antagonist with great pharmaceutical potential) from very long (0.5 $\mu$s) massively parallel molecular dynamics (MD) simulations in full atomistic detail. We extract coarse-grained descriptors of protein shape (ellipsoid), and of translational and rotational mobilities, i.e., the basic components at the lowest hierarchical level in a multiscale modeling strategy. Structural analysis reveals the folded conformation and asymmetric shape to be strongly favored for conotoxin. In accordance with experimental findings, conformational stability is observed and found to be linked to the presence of the α-helix along the 15 residues and to the existence of the two disulfide bonds. We find rotational ($D_r$) and translational ($D_t$) diffusivities to be suitable descriptors of coarse-grained dynamics, i.e., of the hydrodynamic behavior, and obtain $D_r = 3.62\ (\pm 0.17) \times 10^8\ s^{-1}$ and $D_t = 1.08\ (\pm 0.4) \times 10^{-10}\ m^2\ s^{-1}$. We further compare the MD-computed coarse-grained descriptors with first principles theoretical predictions based on the extended Hess−Doi Fokker−Planck approach which relates particle shape and dimensions to diffusion coefficients. An excellent agreement between simulation data and analytical predictions is observed for both dynamical descriptors. This comparison strongly suggests that diffusivities of rigid biomolecules much larger than the α-conotoxin AuIB studied here can be obtained from the coarse-grained shape descriptor (ellipsoid) derived from relatively short MD simulations.

For personal use only. No commercial redistribution.

## I. Introduction

Recent developments on the experimental studies of protein/liquid crystal (LC) interaction have shown that the adsorption of single biological molecules at interfaces can be detected through the use of anchoring transitions in liquid crystals, thereby providing the basis for fast and inexpensive biological sensors.[1−7] In a prototypical application, a sensing device operates based on the observation that a phospholipid-laden interface between a liquid crystal phase and an aqueous phase gives rise to an homeotropic (perpendicular) anchoring of the liquid crystal at the interface. Upon addition of proteins to a flowing aqueous phase, some of the proteins adsorb at the interface and perturb the packing of the lipids and the order of the adjacent liquid crystalline phase, giving rise to anchoring transitions and a concomitant formation of defects. The defects are amplified over length scales of nanometers to microns, and can therefore be detected by simple optical means.[2,6,7] The design of such a sensor requires considerable trial-and-error experimentation and optimization of numerous variables (choice of surfactants and liquid crystal, micro- or nanochannel dimensions, flow rate, etc.). A multiscale modeling formalism capable of describing such systems would be particularly useful in that context. It is known that the orienting influence the protein analyte exerts on the LC phase is strongly dependent, among other things, on protein shape.[6] The same strong shape dependence has also been observed for anisotropic reactivity on the rate of diffusion-controlled reactions.[8,9] Additionally, the sensitivity and response time of the sensor are directly coupled to the mobility of the protein in the aqueous phase, i.e., on how rapidly it can reach the water/LC interface. Hence, it is necessary, at the lowest hierarchical level of the multiscale formalism, to carry out a reliable and systematic coarse-graining of protein shape and dynamics in the aqueous phase.

At higher hiearchical levels, questions such as how the anchoring transition (binding of the protein to the interface) that occurs on the length scale of a few nanometers is amplified over macroscopic length scales must be addressed. Once this amplification mechanism is understood, multiscale theory and simulation can be used to conceive protein/LC systems with optimal sensing capabilities. The principle can be extended to the design of elegant and highly effective biosensors for detection of proteins, viruses, and cells.

In this contribution, we present an atomistic modeling study of protein shape, size, and mobility in an aqueous phase, and their coarse-grained structural and dynamic description. We have selected α-conotoxin AuIB as the model protein, due to its favorable shape stability characteristics and also due to its practical relevance as an analyte. Furthermore, its moderate size is a convenient characteristic, since we have found that a reliable description/coarse-graining of the diffusive behavior entails very long and large-scale molecular dynamics (MD) simulations. In addition, such small, disulfide-rich peptides found in the poison of the *Conus* species have attracted considerable scientific interest during past years mainly due to their great potential in

* To whom correspondence should be addressed. E-mail: mlaso@etsii.upm.es.

10.1021/jp806734c CCC: $40.75 © 2009 American Chemical Society
Published on Web 03/23/2009

related contributions available from the author(s) at www.complexfluids.ethz.ch

the areas of pharmacology and especially in neurochemistry and neurobiology.[10–20] Specific *Conus* peptides target different neuronal receptors, primarily ligand-gated and voltage-gated ion channels.[17,19] For example, the nicotinic acetylcholine receptor (nAChR), a nonselective pentameric ligand-gated cation channel can be specifically inhibited by the α-conotoxin family of peptides.,[13,19,21−24] $\kappa$-, $\mu$-, and $\omega$-Conotoxins block potassium ($K^+$), sodium ($Na^+$), and calcium ($Ca^{2+}$) voltage-gated channels, respectively.[17,19] Among other examples of target selectivity, the $\rho$-conotoxins block α1-adrenoceptors,[14] the $\chi$-family inhibits noradrenaline transporters,[25] and the 5-HT3 serotonin-gated ion channel is rendered inactive by the $\sigma$-conotoxin GVIIIA.[26]

The disulfide-rich conotoxins usually consist of 10−30 amino acids, which may be cross-linked, most often by two to three disulfide bonds. These disulfide bridges typically lead to compact molecular conformations. Conotoxins are very water-soluble and stable with solution conformations that are invariably constrained by the presence of the disulfide links and/or of an α-helix.[17] From the modeling perspective, all the aforementioned features render them excellent candidates for detailed atomistic simulations since their size and consequently their segmental and global dynamics in solution are within the reach of state-of-the-art, massively parallel computational techniques. A particularly attractive application of such tools is the in silico modification of the connectivity of the disulfide links of the computer-generated conotoxins to analyze its effect on the biological activity of the peptide, a study that requires the chemical synthesis of conopeptide variants,[27] accompanied by a molecular-level comparison between different members of the same superfamily to identify the structure−activity relationship.[28] The chemical synthesis of substituted protein motifs may become a nontrivial, expensive procedure. Computer simulations can greatly assist experimental efforts toward this direction and can be further benefited through comparison/validation with experimental data.[29−31] Atomistic modeling investigations of conopeptides have started to appear in the literature in the past 10 years. The NMR structure of α-conotoxin MI in water has been refined by Gouda et al.[32] through molecular dynamics (MD) simulations of relatively short duration (hundreds of picoseconds) using an all-atom model for the toxin and the water molecules. In a recent simulation, Dutertre and Lewis[33] performed a modeling investigation of the interactions between α-conotoxins and neuronal nicotinic receptors (nAChRs), while the channel gating in nAChR has been studied by Cheng et al.[34] through targeted molecular dynamics simulations.

The present study focuses on the conformational stability, size, structure, and dynamics of the α-conotoxin AuIB (from *Conus aulicus*) in water. Simulation results to be presented have been extracted from massively parallel, detailed atomistic MD trajectories, each of 0.5 $\mu$s duration, on four different and statistically uncorrelated model samples. Section II provides a brief analysis of the simulated peptide and all technical details regarding force field and simulation parameters. Section III offers insight about the conformational stability of the conopeptide and the corresponding mobility of the constituent residues, and it analyzes the effect of the existing disulfide bonds on stability. Section IV is devoted to the analysis of protein dimensions and conformation, and of the time evolution of shape and size coarse-grained descriptors. Section V collects our atomistic simulation results for the conotoxin dynamics, the extraction of the corresponding coarse-grained descriptors, and comparison with analytic expectations based on the extended Hess−Doi Fokker−Planck model. Finally, the paper closes with the major conclusions and findings, as well as a discussion of potential applications for conotoxins including the computer-aided design of (a) ultrasensitive biosensors and of (b) nonaddictive pharmaceutical drugs.

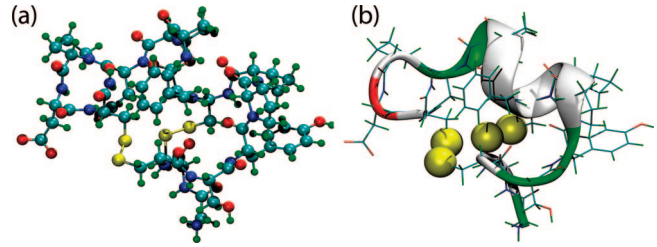


**Figure 1.** α-Conotoxin AuIB (1DG2) shown in (a) CPK representation where atoms and bonds are shown as spheres and cylinders, respectively, and (b) cartoon representation where residues are colored according to their type (red, acid; green, polar; white, nonpolar). In the latter representation the two pairs of sulfur atoms forming disulfide bridges are depicted as van der Waals spheres.

## II. Systems Studied: Simulation Details

The α-conotoxin AuIB[35,36] (PDB ID: 1DG2) is a 15-residue, $NH_2$-terminated disulfide-rich peptide from the venom of *Conus aulicus*. It belongs to the A-superfamily of conotoxins with potential pharmacological applications as it targets neuronal nicotinic acetylcholine receptors. The complete sequence of the constituent amino acids, as identified by Luo et al.,[37] is GCCSYPPCFATNPDC*, where the asterisk indicates an amidated terminus.[27,38] It bears two disulfide bridges, which are single covalent bonds that connect the thiol groups, between the following cysteine (Cys) pairs: (i) residues 2 and 8, and (ii) residues 3 and 15. The characteristic pattern of the Cys amino acids along 1DG2 is $CCX_mCY_nC$.[39] According to the amino acid sequence, $m = 4$ and $n = 6$; consequently, α-conotoxin AuIB belongs further to the α4/6 (α$m$/$n$) subgroup of the α-family. Besides the presence of the two disulfide bridges, the conformation of 1DG2 is further constrained by the existence of an α-helix leading to a 40% helical conformation of the secondary structure.

Sequence details, structural data, and corresponding atomic coordinates were obtained from the RCSB (Research Collaboratory for Structural Bioinformatics) Protein Data Bank (PDB),[40] as obtained from the experimental NMR measurements of Cho et al.[38] In case of missing heavy atoms in the toxin configuration of the corresponding PDB file, identity and coordinate guesses were based on a residue-type identification algorithm through the VMD (Visual Molecular Dynamics)[41,42] molecular graphics/analysis program. Figure 1 presents α-conotoxin AuIB in (a) CPK representation where atoms are depicted as spheres of scaled-down van der Waals (vdW) radius and bonds as cylinders, and in (b) cartoon representation with residues colored according to type. Also shown in Figure 1b as vdW spheres are the pairs of the sulfurs of the two disulfide bonds present in the molecule.

All present MD simulations were executed using the NAMD (Nanoscale Molecular Dynamics)[43,44] molecular dynamics software. In the past NAMD has been shown to take full advantage of supercomputing facilities for simulations of large biological systems.[45–47] In the present work, all reported simulations were executed in parallel spanning from 16 up to 64 CPUs.

All bonded and nonbonded potential interactions between atoms were described by the CHARMM (Chemistry at Harvard Macromolecular Mechanics)[48,49] all-atom force field (update 31b1), while water molecules were represented explicitly through the TIP3P model[50] as implemented in CHARMM. For

For personal use only. No other reproduction.

related contributions available from the author(s) at www.complexfluids.ethz.ch

**TABLE 1: Equilibration Cycle Adopted for the Preparation of Four Statistically Different Initial Configurations for α-Conotoxin AuIB in Water**

| step | duration | details |
|---|---|---|
| energy minimization | 50 000 iterations | |
| NPT MD | 100 ps | protein atoms held fixed in space; $T = 305$ K, $P = 1$ atm |
| energy minimization | 100 000 iterations | |
| NVT MD | 200 ps | $T = 305$ K |
| energy minimization | 100 000 iterations | |
| NPT MD | 200 ps | $T = 305$ K, $P = 1$ atm |
| NVT MD[a] | 200 ps | $T = 305$ K |
| NPT MD[a] | 500 ps | $T = 305$ K, $P = 1$ atm |

[a] The final two steps are modified by intercalating energy minimizations to obtain four, statistically independent, fully relaxed configurations.

short-range, nonbonded interactions a cutoff distance was set at 12 Å. A smooth switching function was adopted for the truncation of the van der Waals potential for the interval 10 Å $\leq r \leq$ 12 Å, where $r$ is the distance between the pair of interacting sites. Furthermore, a pair neighbor list at 14 Å allowed for a significant speed-up in the calculation of nonbonded interactions. Coulombic interactions were calculated through the PME (particle mesh Ewald)[51] full-electrostatics method. Partial charges for all atoms were assigned based on the force-field type according to CHARMM. No scaling factor was adopted for the electrostatic interactions between intramolecular pairs separated by three bonds. In all simulations time integration was performed by a multiple-time-step algorithm in which only bonded interactions and short-range nonbonded ones were calculated at every "small" time step, $\delta t_1$, whereas the long-range electrostatics were calculated only every "large" time step $\delta t_2$. In all MD simulations reported here the values $\delta t_1 = 2$ fs and $\delta t_2 = 4$ fs were used. Lengths of all bonds involving hydrogen atoms were held fixed through the ShakeH algorithm[52,53] with a convergence tolerance set to $10^{-8}$ Å. All production runs were cast in the isothermal−isochoric (NPT) ensemble ($T = 305$ K, $P = 1$ atm) using a modified Nosé−Hoover algorithm with Langevin dynamics for the both system barostat and thermostat.[54,55] Langevin temperature coupling was applied to all atoms except hydrogens, with the damping coefficient being set at 5 $ps^{-1}$. For pressure control, isotropic cell fluctuations were coupled to a piston with period and decay times of 200 and 100 fs, respectively.

Periodic boundary conditions were applied in all three dimensions of the orthogonal simulation cell. Explicitly detailed protein structures were placed in a preequilibrated simulation box filled with water molecules in an energetically favorable way. The simulation cell was subjected to a series of static energy minimizations (MM) and short NPT/NVT MD equilibration runs to ensure structural relaxation and conformational stability of the protein before embarking on the long NPT MD production runs. Furthermore, the final steps of the equilibration cycle were properly modified to produce four different atomistic configurations of conotoxin in water serving as starting points of the four uncorrelated long MD trajectories. Table 1 summarizes the equilibration cycle and the corresponding MM or MD steps together with their duration and specific simulation details.

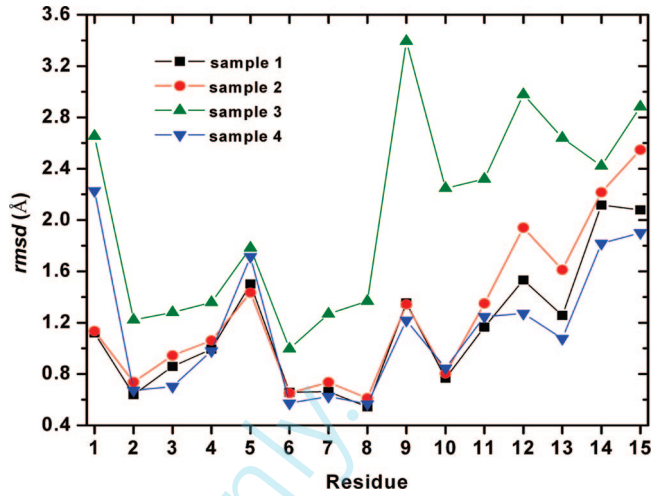


**Figure 2.** Root-mean-square deviation, rmsd, for each individual residue from 500-ns-long NPT MD simulations on four different samples of α-conotoxin AuIB (1DG2) in water.

During the production NPT MD runs, molecular configurations and energy-related statistics were recorded every 0.05 ns. Total simulation time for each of the four independent trajectories was 0.5 μs, for a total cumulated simulation time of 2.0 μs.

## III. Conformational Stability

The conformational stability of the simulated conopeptide over time is quantified through the evolution of the root-mean-square deviation (rmsd) defined as

$$\mathrm{rmsd}(t) = \sqrt{\frac{\sum_{j=1}^{N_{\mathrm{res}}} \sum_{i=1}^{N_{\mathrm{at}}(j)} (\mathbf{r}_i^j(t) - \mathbf{r}_i^j(0))^2}{n_{\mathrm{at}}}} \qquad (1)$$

where $N_{\mathrm{res}}$ is the total number of residues of the toxin (15 for α-conotoxin AuIB), $N_{\mathrm{at}}(j)$ is the total number of atoms of residue $j$, $n_{\mathrm{at}}$ is the total number of atoms over all residues, and $\mathbf{r}_i^j(t)$ is the position vector of atom $i$ of residue $j$ at time $t$. All reported deviations are calculated with respect to the position vector of atoms at $t = 0$[56] and by averaging only over all heavy atoms (i.e., contributions from hydrogen atoms are excluded from eq 1). The root-mean-square deviation is a particularly useful measure of molecular stability since by superimposing successive configurations of the simulated peptide we are able to detect any structural transitions of the constituent residues.

It was found that toxin conformations from all different MD trajectories remain stable within the whole 500-ns-long simulation time, with the rmsd being on average around 1−2 Å. For one of the trajectories, partial unwrapping of the α-helix (as will be further shown and explained below) was observed. The rmsd as global measure of stability can be particularized to individual residues by eliminating the summation over residues in eq 1 in order to identify the most and least constrained residues of the polypeptide. The root-mean-square deviation of each individual residue of the α-conotoxin (AuIB) is given in Figure 2 for four different modeled samples. In this figure averaging for each residue is performed over all recorded time

For personal use only. Not for redistribution

related contributions available from the author(s) at www.complexfluids.ethz.ch

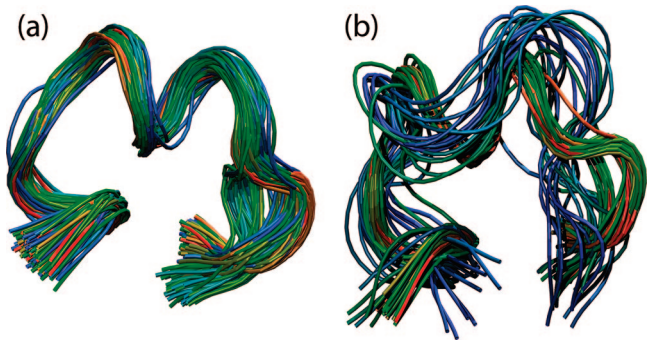


**Figure 3.** Tube representation of the α-conotoxin AuIB structure colored according to the time step for (a) sample 1 and (b) sample 3. An RGB (red−green−blue) color scheme is used, with red, green, and blue corresponding to time instances near the start, middle, and end of the trajectory, respectively.

instances. The particularly low values of the rmsd of individual residues and the convergence to very similar intensities for the whole amino acid sequence are clear indicators of configurational stability. Even for sample 3, for which the 3-10 helix undergoes partial unraveling, the median rmsd is approximately 2.1 Å. As expected, conformational stability is enhanced in the residues of the α-helix (sequence 6−11) and the cysteine ones (2, 3, and 8) since their thiol groups form the two constraining disulfide links. The last cysteine amino acid (15) of the pair that forms the second disulfide bond exhibits a comparatively large rmsd as it resides in the more flexible, terminal part of the peptide. The great conformational stability of the toxin is best grasped with the help of a tube representation (Figure 3) that very intuitively displays the superimposed secondary structure of the protein backbone at various time instances.

## IV. Conotoxin Shape and Size

The presence of disulfide bonds among the constituent amino acids of conotoxins plays a critical role for the conformational stability and for the predominance of folded and constrained molecular configurations as demonstrated in section III. Consequently, the distribution of the bond lengths of the two pairs of disulfide links, ensemble-averaged over all configurations and all different samples, is very narrow, spanning the small interval [1.90 Å, 2.15 Å] with a modal value at 2.03 Å, typical of the stiff harmonic potential governing bond lengths.

The mean square radius of gyration $\langle R_g^2 \rangle$ is a robust and global coarse-grained descriptor of molecular size, and its evolution in time can provide significant insights regarding the conformational stability of the toxin molecule. Such results as obtained from present MD simulations on all four samples are shown in Figure 4. For trajectories in which the helix retains its conformational stability (i.e., the entire samples 1−4 up to times $t \approx 326$ ns) $\langle R_g^2 \rangle$ adopts an equilibrium value of approximately $\langle R_g^2 \rangle = 38.2 \pm 1.0$ Å$^2$ (one standard deviation in the mean). In addition, fluctuations around it are very small (2 Å$^2$). This is not unexpected since contributions from all residues are taken into account when calculating $\langle R_g^2 \rangle$ and more than half of them are either part of the rigid α-helix or they are constrained by the disulfide bonds. The increase in $\langle R_g^2 \rangle$ for sample 3 at times $t > 330$ ns is due to the partial unwrapping of the α-helix; its unfolded conformation is approximately 20% larger. As seen in Figure 4, the radius of gyration properly reflects the folded−unfolded transition. Consequently, $\langle R_g^2 \rangle$ constitutes a reliable descriptor of overall size and shape stability for α-conotoxin AuIB.

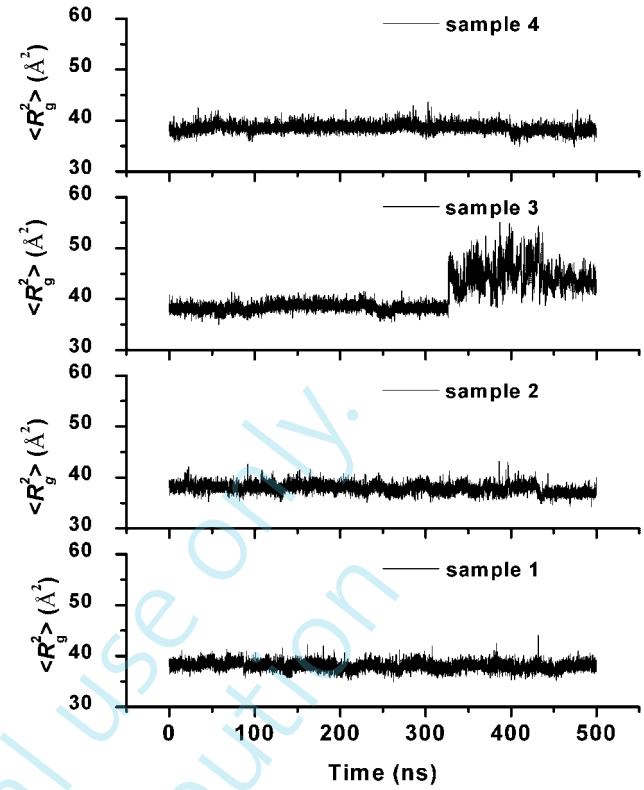


**Figure 4.** Evolution of mean square radius of gyration, $\langle R_g^2 \rangle$, for the four independent trajectories (samples). Partial unfolding of the α-helix (see also Figure 3) is responsible for the increase in $\langle R_g^2 \rangle$ at 330 ns in sample 3.

The scalar $\langle R_g^2 \rangle$ is however unsuitable as a coarse-grained shape descriptor for molecules markedly departing from a spherical shape. For this reason, we have resorted to a descriptor of higher tensorial order for conotoxin, namely the mass inertia tensor relative to the center of mass, **I**. **I** is symmetric by construction; its diagonal elements are the moments of inertia ($I_{xx}$, $I_{yy}$, and $I_{zz}$) and the off-diagonal ones are the products of inertia ($I_{xy} = I_{yx}$, $I_{xz} = I_{zx}$, and $I_{yz} = I_{zy}$) of the molecule. For a molecule consisting of $n_{at}$ atoms (considered as point masses), **I** can be written in dyadic form as[57]

$$\mathbf{I} = \sum_i m_i(\mathbf{r}_i^2\mathbf{1} - \mathbf{r}_i\mathbf{r}_i) \qquad (2)$$

where **1** is the unit dyadic, $\mathbf{r}_i$ and $m_i$ are the position vector and mass of atom $i$, and the summation index $i$ runs over all atoms. Atomic position vectors are calculated with respect to the center of mass of the molecule. In the reference system of the principal axes of inertia, **I** is diagonal. Its three real eigenvalues $I_1$, $I_2$, and $I_3$ correspond to the principal moments of inertia, and the three normalized eigenvectors define a principal axis system ($\mathbf{e}_1$, $\mathbf{e}_2$, $\mathbf{e}_3$), which is co-moving with the molecule and has to be determined at each step from the instantaneous individual atomic coordinates. Special care must be exercised to ensure proper continuity of axis labeling from one time step to the next, i.e., to avoid swapping identities among axes. Maintaining axis continuity is crucial when major conformational changes such as helix unwrapping take place. Otherwise, spurious dynamics result, as reflected in abnormally high rotational diffusivity. For α-conotoxin AuIB we find the eigenvalues $I_1$, $I_2$, and $I_3$ of the mass moment of inertia tensor in all four NPT MD trajectories to be clearly separated during the entire duration

For personal use only. Not for redistribution

related contributions available from the author(s) at www.complexfluids.ethz.ch

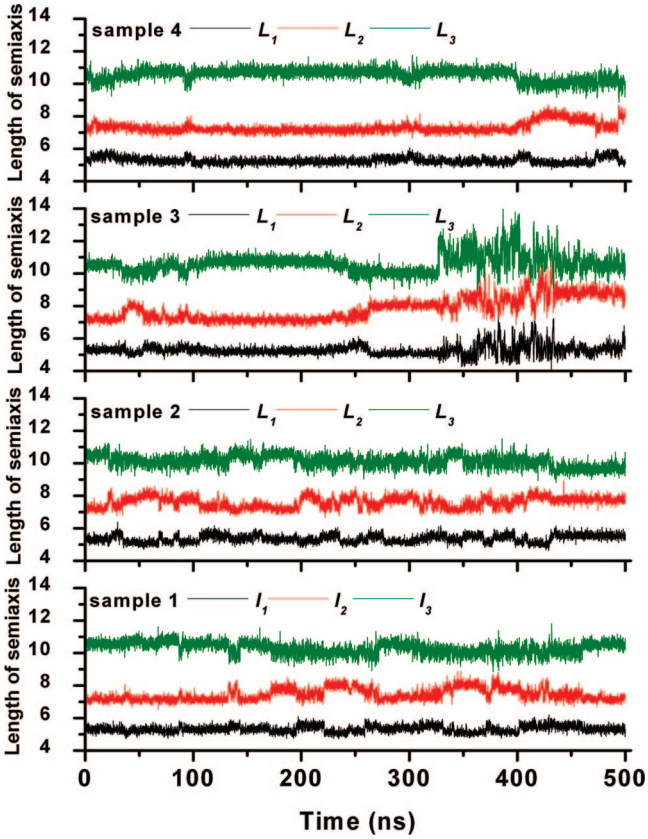


**Figure 5.** Lengths (in angstroms) of the semiaxes of the coarse-grained descriptor (ellipsoid of uniform mass distribution and same principal moments of inertia as the α-conotoxin AuIB) as a function of time, as obtained in four independent NPT MD runs.

of the simulations, indicating a truly triaxial, i.e., nonspherical, and nontransversally axisymmetric shape. The ratios between the moments $I_1/I_2 = 1.20$ and $I_1/I_3 = 1.94$ remain almost constant. The observed separation of $I_1$, $I_2$, and $I_3$ makes it possible to univocally define, as a coarse-grained descriptor of conotoxin shape, an ellipsoid of uniform density that has the same moments of inertia as the conotoxin.[58] The lengths of its semiaxes are given by

$$L_1 = \sqrt{\frac{5}{2}\frac{1}{\sum_{i=1}^{n_{at}} m_i}(I_2 + I_3 - I_1)} \qquad (3)$$

and similarly with $L_2$ and $L_3$ under cyclic permutation of the indices. The evolution of the ellipsoid semiaxes for all trajectories is shown in Figure 5. The ellipsoid inherits the asymmetry of the moment of inertia tensor, so its three axes differ significantly: $L_3 = 10.3$ Å, $L_2 = 7.45$ Å, and $L_1 = 5.31$ Å. Figure 5 clearly shows that ellipsoid semiaxes, although fluctuating, remain well-defined and, furthermore, that the inequality $L_3 > L_2 > L_1$ holds strictly. The latter implies not only that the overall size (radius of gyration) of α-conotoxin AuIB in water is very stable, but that its overall (coarse-grained) shape remains virtually unchanged. The simulated conotoxin can be thus characterized as remarkably rigid, with virtually constant aspect ratios among its three principal axes. Its coarse-grained shape diverges markedly from a sphere, and it is neither an oblate nor a prolate, but a scalene ellipsoid ($L_1 \neq L_2 \neq L_3$). Figure 6 depicts the coarse-grained scalene ellipsoid, together with the

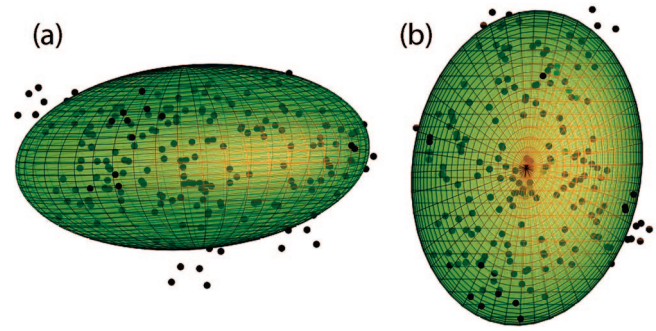


**Figure 6.** Coarse-grained representation as a scalene ellipsoid with dimensions equal to the lengths of the semiaxes (see Figure 5). Atoms of the parent atomistic α-conotoxin AuIB molecule are shown as small black spheres of equal radius, independent of atom type.

atoms of the conotoxin molecules, both at the same scale, with the latter shown as small spheres of equal radius, independently of atomic weight.

## V. Conotoxin Dynamics

The highly complex detailed dynamics of α-conotoxin AuIB at infinite dilution in water can be described at a coarse-grained level by separating it into two simultaneous Brownian motions, a rotational one and a translational one. Rotational motion corresponds to the random motion of an arbitrary unit vector rigidly tied to the diffusing molecule, for example, one of the principal eigenvectors of the mass inertia tensor.[59] At short times the random motion of the tip of $\mathbf{e}_1$ (principal eigenvector, its application point considered to be at the origin) can be regarded as a Brownian motion on a two-dimensional flat surface with the rotary diffusivity $D_r$ given by[59]

$$D_r = \frac{\langle(\mathbf{e}_1(t) - \mathbf{e}_1(0))^2\rangle}{4t} \qquad (4)$$

where $\langle(\mathbf{e}_1(t) - \mathbf{e}_1(0))^2\rangle$ is the mean square displacement of the tip of vector $\mathbf{e}_1$ at time $t$ with respect to the time origin ($t = 0$). The precise meaning of "short times" in the previous paragraph is that $D_r t \ll 1$, so the curvature of the two-sphere manifold $|\mathbf{e}_1(t)| = 1$ in which diffusion takes place can be neglected. Alternatively, the diffusivity can be computed from the vector correlation function, $\langle\mathbf{e}_1(t)\cdot\mathbf{e}_1(0)\rangle$, which is related to $D_r$ through[59]

$$\langle\mathbf{e}_1(t)\cdot\mathbf{e}_1(0)\rangle = \exp(-2D_r t) \qquad (5)$$

Additionally, a characteristic rotational correlation time can be defined in terms of $D_r$ as[59]

$$\tau_r = \frac{1}{2D_r} \qquad (6)$$

(other definitions, differing only by a constant factor in the denominator, are also in use), and consequently $\tau_r$ can be extracted from the $\langle\mathbf{e}_1(t)\cdot\mathbf{e}_1(0)\rangle$ vs $t$ curve by fitting eq 5 at short times.[60]

The decay of the autocorrelation function $\langle\mathbf{e}_1(t)\cdot\mathbf{e}_1(0)\rangle$ is shown in Figure 7 for all individual samples, as well as for the average over the four trajectories using multiple time origins.[53] While the evolution of $\langle\mathbf{e}_1(t)\cdot\mathbf{e}_1(0)\rangle$ for each sample shows strong fluctuations characteristic of individual instances of a stochastic

For your personal use only. Not for redistribution

related contributions available from the author(s) at www.complexfluids.ethz.ch

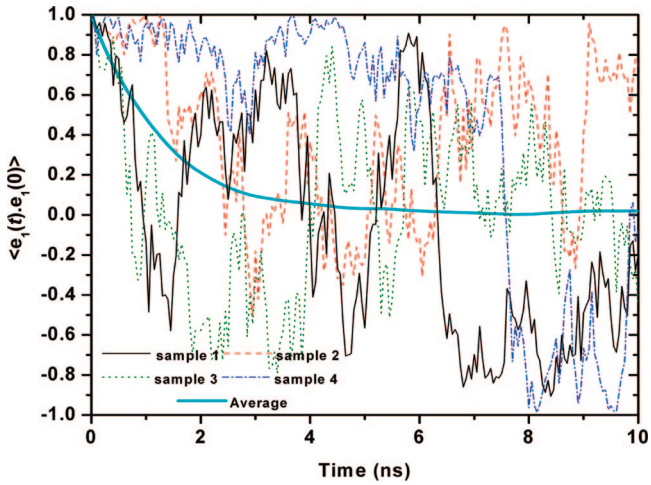


**Figure 7.** Evolution in time of the instantaneous value of the vector correlation function $\langle \mathbf{e}_1(t)\cdot\mathbf{e}_1(0)\rangle$ as obtained from NPT MD simulations on the four samples of α-conotoxin AuIB in water. Also shown is the corresponding curve as obtained from averaging over all samples and by employing multiple time origins (running average values).

process, averaging $\langle \mathbf{e}_1(t)\cdot\mathbf{e}_1(0)\rangle$ over four samples is sufficient to obtain a smooth evolution, from which $D_r$ can be obtained by simple least-squares fitting as a free parameter in eq 5. This way, a value of $D_r = 3.62\ (\pm 0.17) \times 10^8\ s^{-1}$ is found for the rotary diffusivity of α-conotoxin AuIB in water. The rotational correlation time of $\tau_r = 1.38$ ns indicates that, from the point of view of rotational dynamics, subtrajectories of a length $\simeq 4\tau_s = 5.5$ ns are fully decorrelated. Compared to the total simulation time (500 ns) the rotational correlation time is smaller by a factor of about 90 for each sample. MD runs of up to 10 ns are thus more than sufficient to accurately determine rotational dynamics of α-conotoxin AuIB in water at room temperature. Hence, the rotary diffusivity of α-conotoxin AuIB in water and rotational correlation time are calculated with very high accuracy through the present MD simulations.

While rotational relaxation can be captured within relatively short times, considerably more effort is required for the accurate estimation of translational diffusivity, $D_t$, since it is only in the long-time, Fickian limit that $D_t$ can be calculated from the mean square displacement of the protein center of mass according to the Einstein equation:

$$D_t^E = \lim_{t\to\infty} \frac{\langle (\mathbf{r}_{cm}(t) - \mathbf{r}_{cm}(0))^2 \rangle}{6t} \qquad (7)$$

where $\mathbf{r}_{cm}(t)$ denotes the position vector of the center of mass of the toxin at time $t$. Figure 8 presents the instantaneous and running average values of the center-of-mass mean square displacement, $\langle (\mathbf{r}_{cm}(t) - \mathbf{r}_{cm}(0))^2 \rangle$, as a function of time in log−log plots for all four samples. Variability in toxin mobility among the samples is substantial, clearly indicating that estimating translational diffusivity as accurately as rotational diffusivity is by no means trivial. The number and length of independent trajectories were actually determined by the need to obtain a reliable value for $D_t$. The most critical condition for the accurate determination of the conotoxin diffusivity is that the duration of the simulation time is long enough to ensure that Fickian diffusion is well established. Otherwise, anomalous diffusion that prevails for short-time scales may pollute the calculation of transport properties. In order to ensure that the Einsteinian diffusive regime has been reached, for all simulated samples,

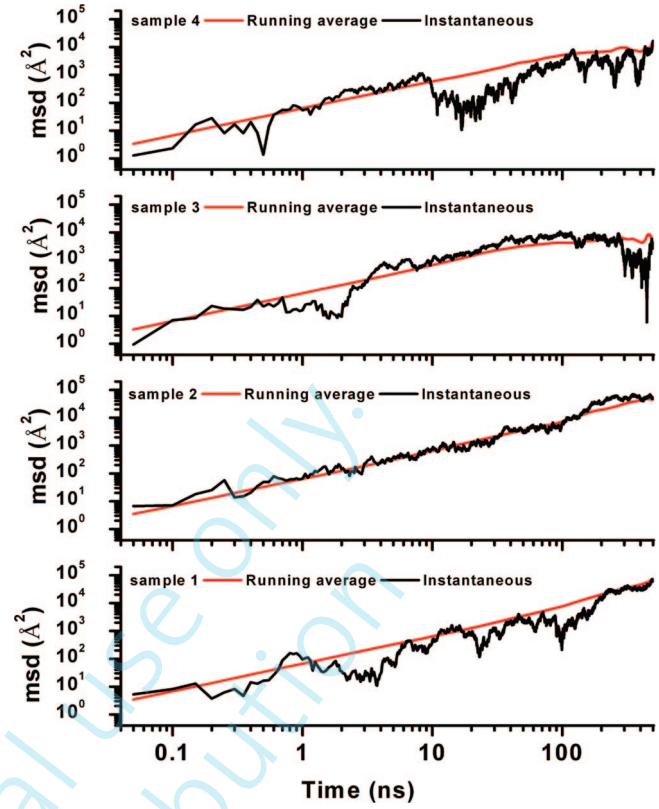


**Figure 8.** Running average and instantaneous values of the mean square displacement (msd) of the toxin center of mass as a function of time in logarithmic scale as obtained from NPT MD simulations on the four samples of α-conotoxin AuIB in water.

the mean square displacement of the molecule was at least one order of magnitude larger than the molecule size as quantified by the mean square radius of gyration. Only by averaging over four independent MD trajectories of 500 ns each, and by incorporating averaging over multiple time origins, could a statistically reliable value $D_t^E = 1.08\ (\pm 0.4) \times 10^{-10}$ m$^2$/s for the translational diffusivity and its uncertainty be obtained.

Alternatively, the (translational) diffusion coefficient can be extracted by the velocity autocorrelation function through the Green−Kubo relation:[53,61]

$$D_t^{GK} = \frac{1}{3}\int_0^\infty \langle \mathbf{v}(t)\cdot\mathbf{v}(0)\rangle\, dt \qquad (8)$$

where $\mathbf{v}(t)$ denotes the velocity vector at time $t$. While eqs 7 and 8 are equivalent for classical systems, the precision of each approach is subject to different factors.[61] For example, in eq 8 the calculation of the integral for large time scales entails significant statistical uncertainty subject to the size of the simulated system.[53] Application of the Green−Kubo relation on all four samples provides a value for the translational diffusivity of $D_t^{GK} = 2.76\ (\pm 1.9) \times 10^{-10}$ m$^2$/s, which is very close to the corresponding estimate from the Einstein equation ($D_t^E = 1.08\ (\pm 0.4) \times 10^{-10}$ m$^2$/s).

It is remarkable that, in spite of the comparatively small size of the molecule, of its shape stability, of being de facto at infinite dilution, and of the very large cumulated simulation time (2 μs), the value of $D_t$ is determined within relatively high statistical uncertainty only. Furthermore, decreasing this uncertainty (linearly) would require longer (quadratically growing) simulation times. Within the current computational resources this is

For your personal use only. Not for redistribution

related contributions available from the author(s) at www.complexfluids.ethz.ch

not readily realizable. The obvious conclusion is that determining the simplest coarse-grained descriptor for translational dynamics via brute force MD for larger biomolecules, or at higher concentrations, or in a medium made up of larger molecules (i.e., a liquid crystal) rapidly becomes unfeasible.

This impasse has motivated us to explore and validate an alternative, analytical method of obtaining coarse-grained estimates for rotational and translational dynamics. The observed shape and size stabilities of the peptide molecule (see sections III and IV) allow a theoretical prediction of rotational and anisotropic translational diffusivities based on the coarse-grained shape of the conotoxin. Theoretical, rigorous expressions for the rotary and translational diffusivities have been developed within the extended Hess−Doi[59,62] Fokker−Planck approach to inhomogeneous nematics. According to Kröger and Ilg,[63] the rotary diffusivity is given by

$$D_r = \frac{3Q\{(2Q^2 - 1)\ln[2Q(Q + \tilde{Q}) - 1] - 2Q\tilde{Q}\}}{4(Q^4 - 1)\tilde{Q}} D_0, \qquad \tilde{Q} = \sqrt{Q^2 - 1} \quad (9)$$

where $Q$ is the ratio of the lengths of the semiaxes for prolate ($Q > 1$) objects and $D_0$ denotes the rotary diffusivity of a sphere of volume equal to that of the ellipsoid (i.e., a sphere of radius $a_0$ equal to $a_0 = (L_1L_2L_3)^{1/3}$). $D_0$ can be readily calculated from[63]

$$D_0 = \frac{k_B T}{\pi n_s a_0^3} \quad (10)$$

where $k_B$ is the Boltzmann constant and $n_s$ is the viscosity of the solvent. Inserting in eq 10 $n_s = 0.001$ Pa·s for water, $T = 305$ K, and $a_0$ as calculated from the lengths of the semiaxes for the coarse-grained ellipsoid of conotoxin (see Figure 5 and related discussion), we obtain $D_0 = 4.04 \times 10^8$ s$^{-1}$. Assuming eq 9 to be valid for a scalene ellipsoid and using the ratio $Q = L_3/L_2$ (or $Q = L_3/L_1$), we estimate the value of rotary diffusivity as $D_r = 3.56 \times 10^8$ s$^{-1}$ (or $D_r = 2.76 \times 10^8$ s$^{-1}$), which compares exceptionally well with the simulation finding of $D_r = 3.62\ (\pm 0.17) \times 10^8$ s$^{-1}$.

Expressions are also available for the translational diffusivity of the scalene ellipsoid as a function of the shape factor $Q$ and the translational diffusivity of a sphere of equal volume, $D_1$. The latter can be approximated as[63]

$$D_1 = \frac{k_B T}{6\pi n_s a_0} \quad (11)$$

Inserting into (11) the parameters for $n_s$, $a_0$, and $T$ described above, we obtain $D_1 = 2.96 \times 10^{-10}$ m$^2$/s for the diffusivity of an isotropic, homogeneous sphere of equal volume. The corresponding expressions for the translational diffusivities parallel, $D_p$, and perpendicular, $D_v$, to the molecular axis are given by[63]

$$D_p = \left(\frac{1 + Q^2}{2Q^{2/3}}\right)\frac{D_r}{D_0} D_1,$$
$$D_v = \frac{3Q^{1/3}}{8}\left[\frac{Q}{\tilde{Q}^2} + \frac{(2Q^2 - 3)\ln(Q + \tilde{Q})}{\tilde{Q}^3}\right] D_1 \quad (12)$$

The isotropic diffusion coefficient, $D_t$, is one-third the trace of the diffusivity tensor:[63]

$$D_t = \frac{D_p + 2D_v}{3} \quad (13)$$

It is this value that can be compared directly with the value that Einstein's (or Green−Kubo's) expression yields for $D_t$ from the MD simulations. Based on the coarse-grained shape descriptors (lengths of the semiaxes) and setting $Q = L_3/L_2$, we obtain $D_t = 2.94 \times 10^{-10}$ m$^2$/s, which is larger than the corresponding value obtained from the Einstein equation (7) in the Fickian limit ($D_t^E = 1.08 \times 10^{-10}$ m$^2$/s) by a factor of approximately 3 and lies very close to the value obtained from the Green−Kubo relation (8) ($D_t^{GK} = 2.76 \times 10^{-10}$ m$^2$/s). We should note that, while the agreement is better in the latter comparison, the calculation of the diffusivity through the velocity autocorrelation function (Green−Kubo) entails a larger statistical error than the corresponding estimate of the Einstein equation in the Fickian limit. It is important to consider that obtaining an estimate of the diffusivity of the correct order of magnitude via MD is a substantial achievement even for small, spherical penetrants,[64−66] let alone large, irregular biomolecules. Besides, a well-known but often overlooked fact is that in practical calculations (e.g., thickness of diffusion boundary layer) the diffusivity invariably appears as the combination $(D_t t)^{1/2}$, so that the impact of any discrepancy in the diffusivity scales only as the square root of the ratio of measured and predicted $D_t$.

The nice agreement between computed and estimated diffusivities suggests that one may quite reliably estimate coarse-grained dynamic descriptors of lethal toxins (for example, anthrax) much larger than the α-conotoxin AuIB studied here from the coarse-grained shape descriptor (ellipsoid of semiaxes $L_1$, $L_2$, and $L_3$), since plateau values of the dimensions are reached very quickly and are hence accessible in relatively short MD simulations. These static shape descriptors, together with solvent viscosity and temperature, can be used to predict rotational and translational diffusivities via eqs 9−13 and related shape-dependent quantities such as rheophoretic and thermophoretic accelerations[67,68] without performing demanding MD.

A final word regarding the decoupling of rotational and translational diffusivities is in order. In the previous sections we have tacitly assumed that both dynamical processes can be treated independently, and that a scalar $D_r$ and a tensorial $D_t$ are proper dynamic descriptors. A more rigorous analysis would deal with both aspects in a unified manner through a mobility matrix. Our assumption is equivalent to ignoring off-diagonal blocks in the mobility matrix, i.e., cross-coupling effects between rotational and translational dynamics. Our decoupling strategy is justified a priori by the large separation of characteristic time scales for rotational $O$(10 ns) and translational $O$(1000 ns) relaxations. It is verified a posteriori by the observed success of eqs 9−13in predicting rotational and translational diffusivities. A strong coupling between both dynamical processes would result in a failure of the extended Hess−Doi approach.[59,62] Although it is perfectly possible to extract the mobility matrix from the instantaneous velocities, forces, and torques, the resulting picture would not deviate appreciably from that obtained under the decoupling approximation, and would introduce unnecessary complications in the coarse-graining procedure. However, for biomolecules that are not as shape-stable as α-conotoxin (AuIB), or that undergo frequent major conformational rearrangements, a coupled rotational/translational approach would be warranted. Toward this direction for

For personal use only. Not to be reproduced

related contributions available from the author(s) at www.complexfluids.ethz.ch

intrinsically unstructured proteins, we refer the interested reader to the method introduced in ref 69, where a structural measure (for example, the radius of gyration) is set as the reference quantity and short MD simulations are performed in order to extract the diffusion matrix. Successively, the diffusion matrix is checked for compatibility with the reference structural quantity which enters the generalized canonical distribution function. If compatibility is established, the structural measure is useful as the reference descriptor; if not, higher modes are required to be taken into account. For rigid molecules, such as the α-conotoxin AuIB studied here, a single mode suffices. More details about the proposed methodology can be found in ref 69.

## VI. Conclusions and Outlook

Static and dynamic descriptors have been derived from a modeling analysis of size, shape, and transport dynamic properties of α-conotoxin AuIB in water, obtained from very long (0.5 $\mu$s), fully atomistic, parallel MD simulations. Thanks to sampling over four different (statistically independent) trajectories, remarkably precise quantitative estimates for rotational and translational diffusivities are obtained. α-Conotoxin AuIB is found to possess a stable configuration and a compact size due to the presence of two disulfide bonds and an α-helix along the peptide backbone. The dimensions, the size, and the anisotropic shape of the biomolecule are quantified by a number of different measures including the radius of gyration and the eigenvalues of the mass moment of inertia tensor. For this conotoxin, rotational diffusivity can be obtained from MD runs as short as a few tens of nanoseconds, while a reliable estimation of the translational diffusivity requires total simulation times on the order of a microsecond. We find that theoretical estimates of diffusivities based on Kröger and Ilg's extension[63] of the Hess−Doi[59,62] approach to inhomogeneous nematics compare favorably with computed values. The implication is that dynamic coarse-grained descriptors (diffusivities) can be obtained from static ones (shape) for complex biological molecules. The applicability of this approach critically depends on the biomolecule possessing a stable shape. Provided this condition is met, diffusivities can reliably be estimated from eqs 9−13. However, the applicability of the present method to flexible proteins or to ones without well-defined structures (intrinsically unstructured proteins) is not guaranteed. Although virtually all proteins will display Fickian diffusive behavior at infinite dilution, and hence well-defined diffusivities, shape descriptors and diffusivities for very flexible or very unstructured proteins will reach their asymptotic values only at very long times, perhaps even beyond what is computationally feasible nowadays. In these cases, it will be impossible to obtain such coarse-grained descriptors from short MD runs, and the present method will not represent any saving of time with respect to the complete MD run. For intrinsically unstructured biomolecules a more general approach should be adopted in the spirit of the time-scale-bridging methodology reported in ref 69.

The stability of α-conotoxin AuIB in water makes it a good candidate for a combined experimental and simulational investigation of its interactions with liquid crystals and lipid bilayers, as discussed in the Introduction, since its spontaneous conformational transitions should be easily distinguishable from those induced by the surrounding structured media.

Further simulations of other conotoxins belonging to the same or to a different superfamily are expected to shed light on how the connectivity of the disulfide bridges and the arrangement of the cysteine amino acids affect their static and dynamic properties. The present ultralong MD investigation revealed precise information about the molecular rigidity and anisotropy, and hydrodynamic transport properties of α-conotoxin AuIB. The results strongly suggest that α-conotoxin AuIB is ideally suited for the modeling of the interactions between shape-stable biomolecules and complex fluid environments including among others protein−ligand interactions and protein aggregation through a systematic coarse-graining. Such investigations are in progress aiming at the design of hybrid biological/synthetic systems with applications in ultrasensitive sensors and nanostructured materials. This work is the first stage (diffusion of the toxin analyte through the aqueous phase toward the water/liquid crystal interface) in an ongoing effort to understand, via modeling, the experimental observations made by Abbott and co-workers, and others (see the Introduction and refs 1−9), on the behavior of biological analytes at the interface between aqueous and liquid crystal phases, which is the basis of a new family of ultrasensitive sensors currently under development.[70]

Additionally, computer simulations can further aid the molecular-level understanding of the ability of specific peptides of the conotoxin family to disrupt neuromuscular communication with potential applications in pharmacology and neuroscience. As an example, ziconotide, the chemically synthesized form of the $\omega$-conotoxin MVIIA, serves currently as a therapeutic nonaddictive analgesic for chronic and intractable pain (commercial name Prialt).[13−15,17,18,71−73]

**Acknowledgment.** Financial support from the European Commission (Project No. NMP3-CT-2005-016375) and CICYT (Project No. MAT2005-25569-E) is acknowledged. We are indebted to Profs. Carlos Aleman and Federico Gago, Dr. David Zanuy, and Dr. Rocio Barrales for many fruitful discussions. Very helpful suggestions and comments by Dr. Eileen Faucher (Columbia University, USA) on the first version of the manuscript are appreciated. Allocations of significant amounts of computational time and resources on the "Magerit" supercomputer of CeSViMa (UPM, Spain) and on the "Palu" supercomputer of CSCS (Switzerland) are acknowledged.

## References and Notes

(1) Brake, J. M.; Abbott, N. L. *Langmuir* **2002**, *18*, 6101.
(2) Brake, J. M.; Daschner, M. K.; Luk, Y. Y.; Abbott, N. L. *Science* **2003**, *302*, 2094.
(3) Brake, J. M.; Mezera, A. D.; Abbott, N. L. *Langmuir* **2003**, *19*, 6436.
(4) Guzman, O.; Kim, E. B.; Grollau, S.; Abbott, N. L.; de Pablo, J. J. *Phys. Rev. Lett.* **2003**, *91*, 235507.
(5) Mohanraj, R.; Wu, H. L. *Sens. Lett.* **2007**, *5*, 538.
(6) Govindaraju, T.; Bertics, P. J.; Raines, R. T.; Abbott, N. L. *J. Am. Chem. Soc.* **2007**, *129*, 11223.
(7) Woltman, S. J.; Jay, G. D.; Crawford, G. P. *Nat. Mater.* **2007**, *12*, 929.
(8) Shushin, A. I.; Barzykin, A. V. *Biophys. J.* **2001**, *81*, 3137.
(9) Schmitz, K. S.; Schurr, J. M. *J. Phys. Chem.* **1972**, *76*, 534.
(10) Miljanich, G. P.; Ramachandran, J. *Annu. Rev. Pharmacol. Toxicol.* **1995**, *35*, 707.
(11) Adams, D. J.; Alewood, P. F.; Craik, D. J.; Drinkwater, R. D.; Lewis, R. J. *Drug Dev. Res.* **1999**, *46*, 219.
(12) Jones, R. M.; Bulaj, G. *Curr. Pharm. Des.* **2000**, *6*, 1249.
(13) Olivera, B. M.; Cruz, L. J. *Toxicon* **2001**, *39*, 7.
(14) Harvey, A. L. *Trends Pharmacol. Sci.* **2002**, *23*, 201.
(15) Terlau, H.; Olivera, B. M. *Physiol. Rev.* **2004**, *84*, 41.
(16) Livett, B. G.; Gayler, K. R.; Khalil, Z. *Curr. Med. Chem.* **2004**, *11*, 1715.
(17) Wang, C.-Z.; Chi, C.-W. *Acta Biochim. Biophys. Sin.* **2004**, *36*, 713.
(18) Miljanich, G. P. *Curr. Med. Chem.* **2004**, *11*, 3029.
(19) Norton, R. S.; Olivera, B. M. *Toxicon* **2006**, *48*, 780.
(20) Livett, B. G.; Sandall, D. W.; Keays, D.; Down, J.; Gayler, K. R.; Satkunanathan, N.; Khalil, Z. *Toxicon* **2006**, *48*, 810.
(21) Dutertre, S.; Lewis, R. J. *Biochem. Pharmacol.* **2006**, *72*, 661.

For personal use only. Not for redistribution.

related contributions available from the author(s) at www.complexfluids.ethz.ch

(22) Millard, E. L.; Daly, N. L.; Craik, D. J. *Eur. J. Biochem.* **2004**, *271*, 2320.
(23) Janes, R. W. *Curr. Opin. Pharmacol.* **2005**, *5*, 280.
(24) Bourne, Y.; Talley, T. T.; Hansen, S. B.; Taylor, P.; Marchot, P. *EMBO J.* **2005**, *24*, 1512.
(25) Sharpe, I. A.; Gehrmann, J.; Loughnan, M. L.; Thomas, L.; Adams, D. A.; Atkins, A.; Palant, E.; Craik, D. J.; Adams, D. J.; Alewood, P. F.; Lewis, R. J. *Nat. Neurosci.* **2001**, *4*, 902.
(26) England, L. J.; Imperial, J.; Jacobsen, R.; Craig, A. G.; Gulyas, J.; Akhtar, M.; Rivier, J.; Julius, D.; Olivera, B. M. *Science* **1998**, *281*, 575.
(27) Dutton, J. L.; Bansal, P. S.; Hogg, R. C.; Adams, D. J.; Alewood, P. F.; Craik, D. J. *J. Biol. Chem.* **2002**, *277*, 48849.
(28) Jin, A.-H.; Brandstätter, H.; Nevin, S. T.; Tan, C. C.; Clark, R. J.; Adams, D. J.; Alewood, P. F.; Craik, D. J.; Daly, N. L. *BMC Struct. Biol.* **2007**, *7*, 28.
(29) Tsai, C. J.; Zheng, J.; Zanuy, D.; Haspel, N.; Wolfson, H.; Aleman, C.; Nussinov, R. *Proteins* **2007**, *68*, 1.
(30) Zanuy, D.; Ropero-Rodriguez, F.; Nussinov, R.; Aleman, C. *J. Struct. Biol.* **2007**, *160*, 177.
(31) Zanuy, D.; Rodriguez-Ropero, F.; Haspel, N.; Zheng, J.; Nussinov, R.; Aleman, C. *Biomacromolecules* **2007**, *8*, 3135.
(32) Gouda, H.; Yamazaki, K.-I.; Hasegawa, J.; Hirono, S. *Chem. Pharm. Bull.* **2001**, *49*, 249.
(33) Dutertre, S.; Lewis, R. J. *Eur. J. Biochem.* **2004**, *271*, 2327.
(34) Cheng, X.; Wang, H.; Grant, B.; Sine, S. M.; McCammon, J. A. *PLoS Comput. Biol.* **2006**, *2*, 1173.
(35) Cruz, L. J.; Gray, W. R.; Yoshikami, D.; Olivera, B. M. *J. Toxicol., Toxin Rev.* **1985**, *4*, 107.
(36) Gray, W. R.; Olivera, B. M.; Cruz, L. J. *Annu. Rev. Biochem.* **1988**, *57*, 665.
(37) Luo, S.; Kulak, J. M.; Cartier, G. E.; Jacobsen, R. B.; Yoshikami, D.; Olivera, B. M.; McIntosh, J. M. *J. Neurosci.* **1998**, *18*, 8571.
(38) Cho, J.-H.; Mok, K. H.; Olivera, B. M.; McIntosh, J. M.; Park, K.-H.; Han, K.-H. *J. Biol. Chem.* **2000**, *275*, 8680.
(39) Loughman, M. L.; Alewood, P. F *Eur. J. Biochem.* **2004**, *271*, 2294..
(40) http://www.rcsb.org/pdb.
(41) Humphrey, W.; Dalke, A.; Schulten, K. *J. Mol. Graphics* **1996**, *14*, 33.
(42) *VMD: molecular modeling and visualization program*, version 1.8.6; Theoretical and Computational Biophysics Group, University of Illinois and Beckman Institute; http://www.ks.uiuc.edu/Research/vmd/.
(43) Kale, L.; Skeel, R.; Bhandarkar, M.; Brunner, R.; Gursoy, A.; Krawetz, N.; Phillips, J.; Shinozaki, A.; Varadarajan, K.; Schylten, K. *J. Comput. Phys.* **1999**, *151*, 283.
(44) *NAMD: parallel molecular dynamics program*, version 2.6b2; Theoretical and Computational Biophysics Group, University of Illinois and Beckman Institute; http://www.ks.uiuc.edu/Research/namd.
(45) Hein, J.; Reid, F.; Smith, L.; Bush, I.; Guest, M.; Sherwood, P. *Philos. Trans. R. Soc., A* **2005**, *363*, 1987.
(46) Adcock, S. A.; McCammon, J. A. *Chem. Rev.* **2006**, *106*, 1589.
(47) Sanbonmatsu, K. Y.; Tung, C.-S. *J. Struct. Biol.* **2007**, *157*, 470.
(48) MacKerell, A. D., Jr.; Bashford, D.; Bellott, M.; Dunbrack, R. L.; Evanseck, J. D.; Field, M. J.; Fischer, S.; Gao, J.; Guo, H.; Ha, S.; Joseph-McCarthy, D.; Kuchnir, L.; Kuczera, K.; Lau, F. T. K.; Mattos, C.; Michnick, S.; Ngo, T.; Nguyen, D. T.; Prodhom, B.; Reiher, W. E.; Roux, B.; Schlenkrich, M.; Smith, J. C.; Stote, R.; Straub, J.; Watanabe, M.; Wiorkiewicz-Kuczera, J.; Yin, D.; Karplus, M. *J. Phys. Chem. B* **1998**, *102*, 3586.
(49) MacKerell, A. D.; Feig, M.; Brooks, C. L. *J. Comput. Chem.* **2004**, *25*, 1400.
(50) Jorgensen, W. L.; Chanfrasekhar, J.; Madura, J. D. *J. Chem. Phys.* **1983**, *79*, 926.
(51) Ewald, P. P. *Ann. Phys.* **1921**, *64*, 253.
(52) Ryckaert, J.-P.; Ciccotti, G.; Berendsen, H. J. C. *J. Comput. Phys.* **1977**, *23*, 327.
(53) Allen, M. P.; Tildesley, D. J. *Computer Simulation of Liquids*; Clarendon: Oxford, U.K., 1987.
(54) Martyna, G. J.; Tobias, D. J.; Klein, M. L. *J. Chem. Phys.* **1994**, *101*, 4177.
(55) Feller, S. E.; Zhang, Y. H.; Pastor, R. W.; Brooks, B. R. *J. Chem. Phys.* **1995**, *103*, 4613.
(56) Alternatively, one could calculate the root-mean-square deviation with respect to the average position vector of each atom (over all recorded instances).
(57) Goldstein, H. *Classical Mechanics*; Addison-Wesley: Reading, MA, 1980.
(58) Tsige, M.; Mahajan, M. P.; Rosenblatt, C.; Taylor, P. L. *Phys. Rev. E* **1999**, *60*, 638.
(59) Doi, M.; Edwards, S. F. *The Theory of Polymer Dynamics*; Clarendon: Oxford, 1986.
(60) Laso, M.; Jimeno, N.; Muneta, L. M.; Müller, M. *J. Chem. Phys.* **2006**, *125*, 244901.
(61) Frenkel, D.; Smit, B. *Understanding Molecular Simulation*; Academic: London, 2001.
(62) Hess, S. *Z. Naturforsch., A* **1976**, *31*, 1034.
(63) Kröger, M.; Ilg, P. *J. Chem. Phys.* **2007**, *127*, 034903.
(64) Karayiannis, N. C.; Mavrantzas, V. G.; Theodorou, D. N. *Macromolecules* **2004**, *37*, 2978.
(65) Raptis, E. T.; Raptis, V. E.; Samios, J. *J. Phys. Chem. B* **2007**, *111*, 13683.
(66) Gestoso, P.; Karayiannis, N. C. *J. Phys. Chem. B* **2008**, *112*, 5646.
(67) Garcia-Ybarra, P.; Rosner, D. E. *AIChE J.* **1989**, *35*, 139.
(68) Kröger, M.; Hütter, M. *J. Chem. Phys.* **2006**, *125*, 044105.
(69) Ilg, P.; Öttinger, H. C.; Kröger, M. *Phys. Rev. E* **2009**, *79*, 011802.
(70) http://www.platypustech.com.
(71) Olivera, B. A. *Mol. Biol. Cell* **1997**, *8*, 2101.
(72) Bowersox, S. S.; Luther, R. *Toxicon* **1998**, *36*, 1651.
(73) Skov, M. J.; Beck, J. C.; de Kater, A.; Shopp, G. M. *Int. J. Toxicol.* **2007**, *26*, 411.

JP806734C

For your personal use only. Not for redistribution

related contributions available from the author(s) at www.complexfluids.ethz.ch